

See discussions, stats, and author profiles for this publication at: <https://www.researchgate.net/publication/263943127>

# Stimuli-Responsive Poly(caprolactone) Vesicles for Dual Drug Delivery under the Gastrointestinal Tract

ARTICLE in BIOMACROMOLECULES · NOVEMBER 2013

Impact Factor: 5.75 · DOI: 10.1021/bm401323x

---

CITATIONS

12

---

READS

47

## 2 AUTHORS:



Bapurao Surnar

Indian Institute of Science Education and Res...

4 PUBLICATIONS 15 CITATIONS

[SEE PROFILE](#)



Manickam Jayakannan

Indian Institute of Science Education and Res...

74 PUBLICATIONS 1,566 CITATIONS

[SEE PROFILE](#)

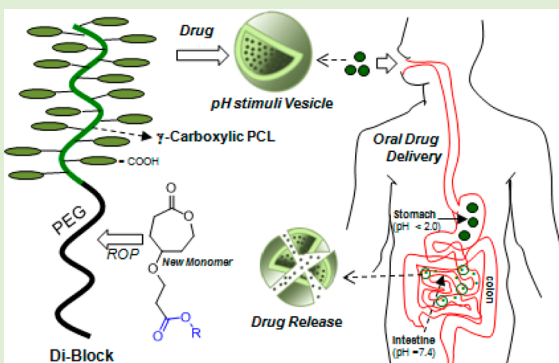
# Stimuli-Responsive Poly(caprolactone) Vesicles for Dual Drug Delivery under the Gastrointestinal Tract

Bapurao Surnar and M. Jayakannan\*

Department of Chemistry, Indian Institute of Science Education and Research (IISER), Dr. Homi Bhabha Road, Pune 411008, Maharashtra, India

Supporting Information

**ABSTRACT:** We report the first example of carboxylic functionalized poly(caprolactone) (PCL) block copolymer vesicles as a novel dual drug delivery pH responsive vehicle for oral administration under the gastrointestinal (GI) tract. A new carboxylic functionalized caprolactone monomer was custom designed through multistep organic reactions and polymerized under controlled ROP using polyethylene glycol (PEG-2000) to produce amphiphilic diblocks, PEG-*b*-CPCL<sub>x</sub>, with *x* = 25, 50, 75, and 100. These carboxylic PCL block copolymers were self-organized into 100–250 nm vesicular assemblies in water. The size and shape of the vesicular assemblies were confirmed by light scattering, zeta potential, and electron microscopes. These vesicles were capable of loading both hydrophilic molecules (Rhodamine B, Rh-B) and hydrophobic drugs such as ibuprofen (IBU) and camptothecin (CPT) in the core and layer, respectively. These pH-responsive PCL vesicles were stable in strong acidic conditions ( $\text{pH} < 2.0$ , stomach) and ruptured to release the loaded cargoes under neutral or basic pH ( $7.0 \leq \text{pH}$ , similar to that of small intestine). The drug release kinetics under simulated GI tract revealed that the individual drug loaded vesicles followed the combination of diffusion and erosion pathway, whereas the dual drug loaded vesicles predominantly followed the diffusion controlled process. Thus, the custom designed PCL vesicles open up new area of pH stimuli responsive polymer vehicles for delivering multiple drugs in oral drug delivery which are yet to be explored for biomedical applications.



## INTRODUCTION

Oral delivery under the gastrointestinal (GI) tract is one of the most elegant methods for the administration of drug molecules with improved patient compliance, low cost, and ease of treatment, and so forth.<sup>1</sup> Oral delivery is a very challenging task because the drug molecules should be stable and retained in the active form under the harsh GI tract and intact against the p-glycoprotein mediated efflux effect.<sup>2</sup> pH-responsive synthetic polymers are particularly attractive for the above purpose since they can protect the drug molecules in the acidic stomach ( $\text{pH} < 2.0$ ) and burst instantaneously under neutral or basic pH ( $7.4$  or  $>7.4$ ) in the small intestine to release the loaded cargoes.<sup>3</sup> Amphiphilic block copolymers,<sup>4</sup> random copolymers,<sup>5</sup> dendronized structures,<sup>6</sup> poly(acrylic acid),<sup>7</sup> polymethacrylic acid,<sup>8</sup> poly(lactic-*co*-glutamic acid),<sup>9</sup> polycarboxylates,<sup>10</sup> amine-functionalized polymers,<sup>11</sup> and poly(trimethylene carbonate)-*b*-poly(L-glutamic acid)<sup>12</sup> are few important examples reported for releasing drugs under pH stimuli. In general, among all of the nano structures, vesicular assemblies are particularly important for drug delivery since they resemble the structure of the cell membrane and also have features for loading both hydrophilic and hydrophobic drugs.<sup>13</sup> Most of the pH stimuli polymer vesicles were employed for administration of DNA,<sup>14</sup> gold nanoparticles,<sup>15</sup> MRI agents,<sup>16</sup> and anticancer drug molecules<sup>6b,8b,17</sup> under *in vitro* conditions similar to that of

intravenous delivery. It is rather surprising to notice that there is no report on pH stimuli polymer vesicles for oral drug delivery under GI tract. Thus, new efforts are required to explore pH stimuli vesicular assemblies for both fundamental understanding as well as developing new scaffolds for oral drug delivery applications.

Poly(caprolactone) (PCL) is one of the most important commercial aliphatic polyesters explored for biodegradable and biomedical applications.<sup>18</sup> PCL is water-insoluble; however, its block copolymer with hydrophilic polyethylene glycol (PEG) chains (PEG-*b*-PCL) provide appropriate hydrophilic and hydrophobic balance to self-organize in water.<sup>19</sup> PEG-*b*-PCL block copolymers were typically known to produce only micelles (not vesicles) for delivering water-insoluble hydrophobic drugs.<sup>19,20</sup> Few reports documented the generation of vesicles based on these block copolymers in a mixed solvent combination of organic + water.<sup>21a,b</sup> Ghoroghchain et al. reported the formation of PEG-*b*-PCL block copolymer vesicles after subjecting these blocks for prolonged reflux in water.<sup>21c</sup> Katz et al. reported TOSUO substituted PEG-*b*-PCL for producing vesicles.<sup>21d</sup> Unfortunately none of these conditions

Received: September 3, 2013

Revised: October 10, 2013

Published: October 15, 2013



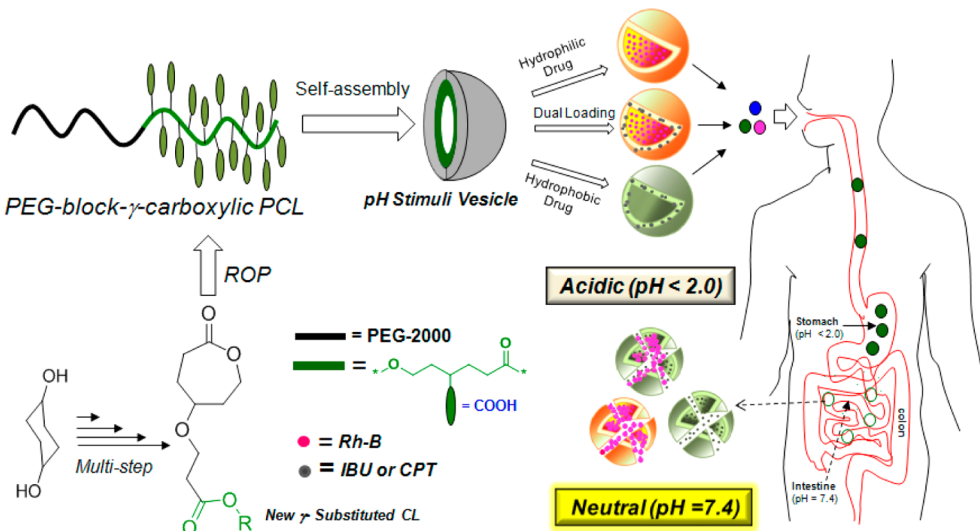


**Figure 1.** Carboxylic substituted PCL block copolymer vesicles and their pH stimuli response delivery under the GI tract.

or approaches are suitable for loading and delivering drugs under pH stimuli. Functional poly(caprolactone)s were also reported having hydroxyl,<sup>22</sup> alkyl,<sup>23</sup> azide,<sup>24</sup> and benzyl<sup>25</sup> or  $\alpha$ -cholesteryl<sup>26</sup> units, and their micelles (or nanoparticles) were employed for drug delivery. Jerome and co-workers reported hydroxyl substituted and click chemistry based  $\alpha$ -position derivatives in poly(caprolactone)s.<sup>27</sup> Hedrick and co-workers had attempted to make carboxylic poly(caprolactone)s; however, it was not successful since the monomer design was only capable of producing low molecular oligomers (no information are available on their molecular self-organization as well).<sup>28</sup> Thus, pH-responsive PCL vesicles are yet to be achieved for drug delivery both in oral and intravenous routes.

The present investigation is emphasized to address the two unresolved problems in polymer drug delivery: (i) design and development of pH responsive PCL block copolymers and (ii) investigation on the individual or dual drug loading and delivering capabilities of pH stimuli PCL vesicular assemblies for oral delivery under GI tract. This new approach is schematically shown in Figure 1. New carboxylic acid substituted caprolactone was synthesized through tailor-made approach and polymerized under controlled ROP to produce series of PEG-block-carboxylic PCL ( $\text{PEG-}b\text{-CPCL}_x$ , with  $x = 25\text{--}100$ ). These new carboxylic functionalized block copolymers were completely water-soluble, and they self-organized into pH responsive polymer vesicles of 100–250 nm in size. These pH stimuli PCL vesicles have unique ability to encapsulate both water-soluble molecules such as Rhodamine-B (RhB) and insoluble anti-inflammatory drug ibuprofen (IBU) and anticancer drugs like camptothecin (CPT). The in vitro release profiles of drug loaded vesicles were studied under stimulated gastrointestinal conditions. The PCL vesicles have stabilized the drug molecules under strong acidic conditions (like pH < 2.0 in stomach) and ruptured to release the cargoes under neutral pH as similar to that of small intestine. Thus, the custom designed PCL vesicles opens up new oral drug delivery approach for pH stimuli polymerosomes, more specifically based on custom designed carboxylic substituted PCL vesicles.

## EXPERIMENTAL METHODS

**Materials.** 1,4-Cyclohexane diol, *t*-butyl acrylate, potassium *t*-butoxide, pyridinium chlorochromate (PCC), metachloroperbenzoic

acid (MCPBA), tin(II) 2-ethylhexanoate ( $\text{Sn}(\text{Oct})_2$ ), triethylene glycol monomethyl ether (TEG), polyethylene glycol monomethyl ether (MW = 2000, here after referred as PEG), caprolactone, Rhodamine B (Rh B), ibuprofen (IBU), and camptothecin (CPT) were purchased from Aldrich chemicals. TEG and PEG were dried under vacuum prior to use. Catalyst  $\text{Sn}(\text{Oct})_2$  and caprolactone were distilled under vacuum and stored in glovebox. All other solvents like tetrahydrofuran (THF) and trifluoroacetic acid (TFA) are purchased locally and distilled and kept under inert atmosphere prior to use.

**Measurements.** NMR was recorded using 400-MHz JEOL NMR spectrophotometer. All NMR spectra were recorded in  $\text{CDCl}_3$  containing TMS as an internal standard. MALDI-TOF of the polymers was determined by using Applied Bio systems 4800 PLUS MALDI TOF/TOF Analyzer. Polymer samples were dissolved in tetrahydrofuran (THF) at 1 mg/mL. 2,5-Dihydroxybenzoic acid (DHB) was used as a matrix. The matrix solution was prepared by dissolving 10 mg in 1 mL of MeOH (or 30% ACN). To aid sample ionization, the MALDI target was prespotted with 2 mg/mL NaI in methanol and allowed to air-dry. The mass of the small intermediate precursors was determined using a HRMS-ESI-Q-time-of-flight LC-MS (SynaptG2, Waters). Gel permeation chromatographic (GPC) analysis was performed using Viscotek VE 1122 pump, Viscotek VE 3580 RI detector, and Viscotek VE 3210 UV-vis detector in tetrahydrofuran (THF) using polystyrene as standards. Thermal analysis of all polymers was done using a TA Q20 differential scanning calorimeter. The instrument was calibrated with indium standards. All of the polymers were heated to melt before recording their thermograms to remove their previous thermal history. Polymers were heated and cooled at 10 °C/min under nitrogen atmosphere, and their thermograms were recorded. The thermal stability of the polymers was determined using Perkin-Elmer thermal analyzer STA 6000 model at a heating rate of 10 °C/min in nitrogen atmosphere. Water contact angle measurements were performed on a GBX model (DIGIDROP contact angle instrument) using Windrop software. Extreme care has been taken in carrying out sessile contact angle measurements to monitor contact angle values within 1 min to avoid the evaporation effects. All contact angle measurements were carried out at room temperature (27 °C) under constant humidity (40–50%). The absorption spectra were recorded using Perkin-Elmer Lambda 45 UV-vis spectrophotometer. The emission studies were done using SPEX Fluorolog HORIBA JOBIN VYON fluorescence spectrophotometer with a double-grating 0.22 m Spex1680 monochromator and a 450 W Xe lamp as the excitation source at room temperature. The excitation spectra were collected at 375 and 420 nm (Pyrene emission wavelength), and the emission spectra were recorded by exciting at the excitation maxima. The Pyrene samples were purged with  $\text{N}_2$  gas for at least 15–20 min prior to photophysical experiments. Dynamic light

scattering (DLS) was done using a Nano ZS-90 apparatus utilizing 633 nm red laser (at 90° angle) from Malvern Instruments. At 90° scattered fluctuations were detected to generate correlation function [ $g^2(t)$ ], from this function diffusion coefficient ( $D$ ) calculated by using the cumulant method. By applying the stock-Einstein equation, the particle diameter was calculated. The reproducibility of the data was checked at least three times using independent polymer solutions. The static light scattering experiment (SLS) was carried out using 3D-DLS spectrometer, from LS Instruments, Switzerland. The instrument consists of a He Ne laser having a wavelength of 632.8 nm attached to a computer using Lab view interface utilizing toluene as a reference. The measurement was performed in autocorrelation mode from 20 to 130° by steps of 5°. FE-SEM images were recorded using a Zeiss Ultra Plus scanning electron microscope. For FE-SEM analysis, the samples were prepared by drop casting on silicon wafers and coated with gold. TEM images were recorded using a Technai-300 instrument by drop casting the sample on Formvar-coated copper grid. The fluorescent micrographs were collected using Carl Zeiss Axiovert 200 microscope.

**Encapsulation in Carboxylic PCL Vesicles.** The detailed procedure is given for Rhodamine-B encapsulation. In a typical experiment, 10 mg of the polymer and 1 mg of Rhodamine-B was dissolved in DMSO (2 mL). Distilled water (8 mL) was added dropwise into the polymer solution, and the mixture was stirred at 25 °C for 12 h. The solution was transferred to a dialysis bag (MWCO = 1000) and dialyzed against large amount of distilled water for 3–5 days. Fresh distilled water replaced periodically to ensure the removal of unencapsulated molecules from the dialysis tube.

The drug loading efficiency (DLE) and drug loading content (DLC) were determined by absorption spectroscopy using the following equations:<sup>13c</sup>

$$\text{DLE}(\%) = \{\text{weight of drug in vesicles}/\text{weight of drug in feed}\} \times 100\%$$

$$\text{DLC}(\%) = \{\text{weight of drug in vesicles}/\text{weight of drug loaded vesicles}\} \times 100\%$$

A similar procedure was followed to encapsulate ibuprofen (IBU) and camptothecin (CPT) using 2 mg of drugs in the feed. Dual loading of Rh-B and IBU was performed using 1 mg of each of these molecules.

**In Vitro Drug Release Studies.** Rh-B, IBU, and CPT loaded vesicles were taken in a dialysis bag (in 3 mL), and they were immersed in a 100 mL beaker and dialyzed at 37 °C with constant stirring. Various pH buffers of 2.0, 4.0, 7.4, and 9.2 are employed for the dialysis studies. Simulated gastric fluid (SGF, 5.47 g HCl, 3.72 g KCl, 1 L water, pH 2) and simulated intestinal fluid (SIF, 8 g NaCl, 0.2 g KCl, 1.44 g Na<sub>2</sub>HPO<sub>4</sub>, 0.24 g KH<sub>2</sub>PO<sub>4</sub>, 1 L water, pH 7.4) were also prepared following a literature report for the released studies.<sup>7</sup> At specific time intervals, 3.0 mL of the dialysate was withdrawn and replaced with an equal volume of fresh buffer. The amount of molecule (or drug) released in each aliquot was measured using absorption spectroscopy to quantify their percentage of cumulative release. Each experiment was triplicated to calculate standard error. Cumulative release (%) =  $C_n \times V_o/m \times 100$ , where  $C_n$  is the amount of loaded cargo in the  $n^{\text{th}}$  sample,  $V_o$  is total volume, and  $m$  is the total amount loaded in vesicles.

**Synthesis of *t*-Butyl-3-((4-hydroxycyclohexyl)oxy)-propionates (1).** 1,4-Cyclohexanediol (20.0 g, 172.0 mmol) and potassium *t*-butoxide (200 mg, 1.78 mmol) were taken in dry THF (200 mL) and stirred for 10 min under nitrogen. *t*-Butyl acrylate (11.0 g, 86.1 mmol) in dry THF (50 mL) was added dropwise, and the reaction mixture was refluxed under dry conditions for 24 h. The solvent was removed by rotavapor, and the content was neutralized with 1N HCl (20 mL). It was extracted with ethyl acetate, and the organic layer was dried over anhydrous Na<sub>2</sub>SO<sub>4</sub>. The solvent was removed to get the product as viscous liquid. It was further purified by passing through silica column using ethyl acetate and petroleum ether (1:10 v/v) as eluent. Yield: 16.7 g (78.4%). <sup>1</sup>H NMR (400 MHz, CDCl<sub>3</sub>) δ ppm: 3.64 (m, 3H, O—CH<sub>2</sub>— and O—CH), 3.29–3.39 (m, 1H, CH—OH), 2.4 (t, 2H, —CH<sub>2</sub>CO—), 1.96–1.81 (m, 4H, OCH(CH<sub>2</sub>)<sub>2</sub>), 1.64–1.32 (m, 4H, CO(CH<sub>2</sub>)<sub>2</sub>), 1.45 (s, 9H, —C(CH<sub>3</sub>)<sub>3</sub>). <sup>13</sup>C NMR (100 MHz, CDCl<sub>3</sub>) δ ppm: 171.08, 80.43,

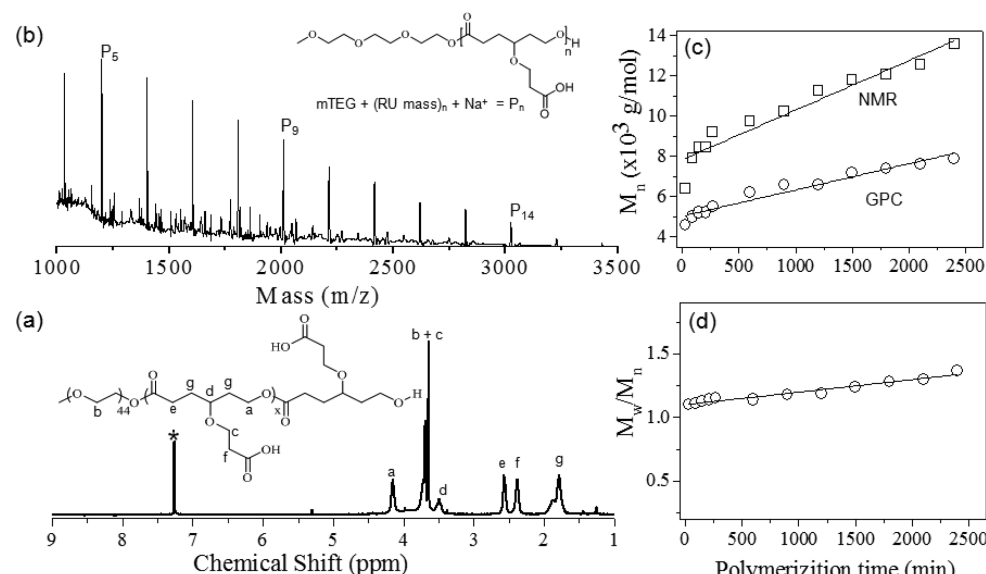
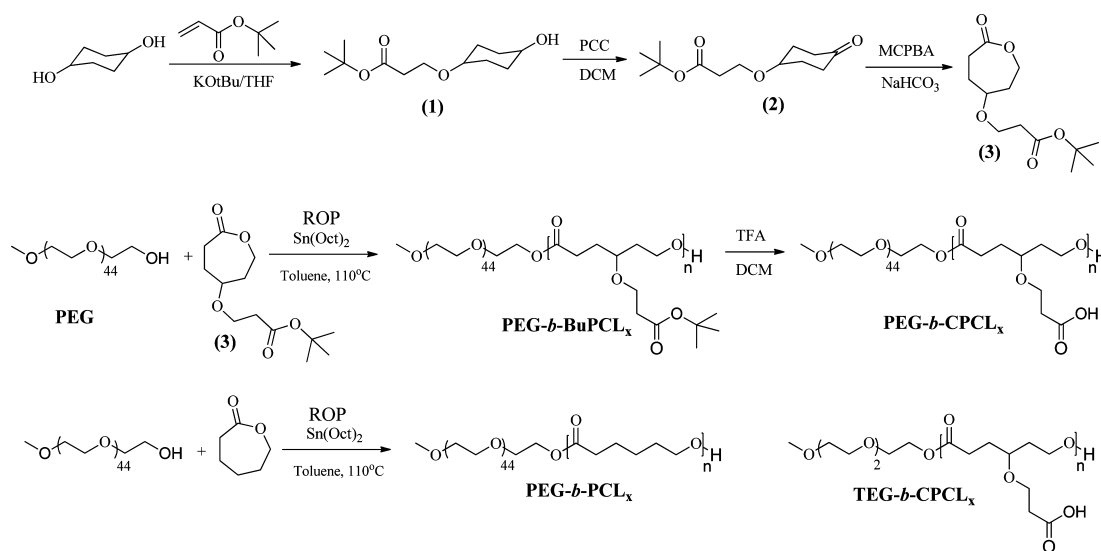
69.50, 63.94, 63.53, 32.54, 30.33, 29.17, and 27.44. FT-IR (cm<sup>−1</sup>): 3421, 2977, 2935, 2863, 1727, 1456, 1393, 1366, 1255, 1155, 1106, and 1034. HR-MS (ESI<sup>+</sup>): *m/z* [M + Na<sup>+</sup>] calcd. for C<sub>13</sub>H<sub>24</sub>O<sub>4</sub> [M<sup>+</sup>]: 267.1572; found: 267.1562.

**Synthesis of *t*-Butyl-3-((4-oxocyclohexyl)oxy)propanoate (2).** PCC (16.7 g, 77.9 mmol) was added to compound 1 (9.5 g, 38.9 mmol) in dry DCM (100 mL) under nitrogen atmosphere, and the reaction mixture was stirred at 25 °C for 4 h. The reaction mixture was filtered through molecular sieves to remove PCC salts. The filtrate was condensed, and the resultant liquid was purified by passing through silica gel column by eluting with petroleum ether/EtOAc (1:4 v/v). The product was obtained as colorless liquid. Yield: 8.5 g (90%). <sup>1</sup>H NMR (400 MHz, CDCl<sub>3</sub>) δ ppm: 3.56 (m, 3H, O—CH<sub>2</sub> and O—CH), 2.58 (t, 2H, —CH<sub>2</sub>—CO), 2.64 (m, 2H, —(C=O)CH<sub>2</sub>—), 2.26 (m, 2H, —(C=O)CH<sub>2</sub>—), 2.09 (m, 2H, —(CO)CH<sub>2</sub>—), 1.90 (m, 2H, —(CO)CH<sub>2</sub>—), 1.45 (s, 9H, —C(CH<sub>3</sub>)<sub>3</sub>). <sup>13</sup>C NMR (100 MHz, CDCl<sub>3</sub>) δ ppm: 211.40, 170.99, 80.56, 72.74, 64.02, 37.02, 36.56, 30.40, and 20.04. FT-IR (cm<sup>−1</sup>): 2974, 2874, 2360, 1716, 1456, 1419, 1393, 1366, 1306, 1249, 1210, and 1100. HRMS (ESI<sup>+</sup>): *m/z* [M + Na<sup>+</sup>] calcd. for C<sub>13</sub>H<sub>22</sub>O<sub>4</sub> [M<sup>+</sup>]: 265.1415; found: 265.1411.

**Synthesis of *t*-Butyl-3-((7-oxooxepan-4-yl)oxy)propanoate (3).** *m*-Chloroperbenzoic acid (3.5 g, 17.3 mmol) was added slowly to a stirred solution of 2 (3.5 g, 14.4 mmol) in dry DCM (40 mL) under nitrogen atmosphere. To the above reaction mixture, anhydrous NaHCO<sub>3</sub> (3.63g, 43.3 mmol) was added, and the reaction was continued at 25 °C for 12 h. The solvent was removed, and the residue was quenched with saturated aqueous NaHCO<sub>3</sub> solution (20 mL) and saturated aqueous Na<sub>2</sub>S<sub>2</sub>O<sub>3</sub> solution (20 mL). It was extracted with ethyl acetate, and the organic layer was dried over anhydrous Na<sub>2</sub>SO<sub>4</sub>. After solvent evaporation, the crude product was purified by passing through silica column using ethyl acetate and petroleum ether (4:6 v/v). Yield = 3.2 g (92%). The product 3 was obtained as colorless liquid. <sup>1</sup>H NMR (400 MHz, CDCl<sub>3</sub>) δ ppm: 4.40 (dd, 1H, COOCH), 4.06 (dd, 1H, COOCH), 3.60 (m, 4H, OCH<sub>2</sub>, OCH, and COCH), 2.98 (dd, 1H, COCH), 2.48 (t, 2H, COCH<sub>2</sub>), 2.42–1.81 (m, 4H, OCH—(CH<sub>2</sub>)<sub>2</sub>), 1.46 (s, 9H, C(CH<sub>3</sub>)<sub>3</sub>). <sup>13</sup>C NMR (100 MHz, CDCl<sub>3</sub>) δ ppm: 176.55, 171.24, 80.99, 74.24, 64.24, 63.66, 36.77, 34.15, 28.40, 27.84, and 27.61. FT-IR (cm<sup>−1</sup>): 2925, 1725, 1456, 1393, 1366, 1253, 1155, 1100, and 1058. HRMS (ESI<sup>+</sup>): *m/z* [M + K<sup>+</sup>] calcd. for C<sub>13</sub>H<sub>32</sub>O<sub>5</sub> [M<sup>+</sup>]: 299.3187; found: 299.3665.

**Ring-Opening Polymerization of Substituted Poly-caprolactone)s.** The typical procedure for ROP was described for substituted caprolactone monomer 3 with [M<sub>0</sub>]/[I<sub>0</sub>] = 100 and polyethylene glycol monomethyl ether as initiator (for polymer PEG-*b*-BuPCL<sub>100</sub>). PEG (31.0 mg, 0.0155 mmol) was taken in a flame-dried Schlenk tube, and dry toluene (1.0 mL) was added under nitrogen atmosphere. To this mixture, Sn(Oct)<sub>2</sub> (3.1 mg, 0.0077 mmol) was added, and the content was stirred at 25 °C for 15 min under nitrogen purge. The monomer 3 (0.4 g, 1.55 mmol) was added to the above mixture, and the polymerization mixture was stirred at 25 °C for 15 min under nitrogen purge. The polymerization tube was immersed in preheated oil bath at 110 °C, and the polymerization was continued for 48 h with constant stirring. The polymerization mixture was precipitated in MeOH. The polymer was redissolved in THF and precipitated again in methanol. The purification was done at least twice to obtain highly pure polymer. Yield: 280 mg (70%). <sup>1</sup>H NMR (400 MHz, CDCl<sub>3</sub>) δ ppm: 4.13 (s, 2H), 3.64 (s, 3.8 H), 3.45 (s, 1H), 3.38 (s, 1H), 2.44 (t, 2H), 2.35 (t, 2H), 1.93–1.81 (m, 2H), 1.81–1.67 (m, 4H), 1.44 (s, 9H, *t*-butyl). <sup>13</sup>C NMR (100 MHz, CDCl<sub>3</sub>): 173.63, 170.81, 80.72, 75.58, 70.68, 65.13, 61.47, 36.60, 33.04, 29.81, 28.86, and 28.22. FT-IR (cm<sup>−1</sup>): 2973, 2931, 1726 (C=O ester), 1457, 1364, 1251, 1156, 1156, 1099, 1062, 957, 898, 845, and 757. GPC molecular weights: M<sub>n</sub> = 18 400, M<sub>w</sub> = 24 900, and M<sub>w</sub>/M<sub>n</sub> = 1.35.

A similar procedure was followed for the synthesis of other compositions of PEG-*b*-BuPCL<sub>x</sub> with x = 25, 50, and 75. Under the identical conditions caprolactone was also polymerized to produce a series of PEG-*b*-PCL<sub>x</sub> with x = 25, 50, 75, and 100. These details are provided in the Supporting Information. Two homopolymers TEG-BuPCL<sub>50</sub> and TEG-PCL<sub>50</sub> (these are not block copolymers) were also synthesized using triethyleneglycol monomethyl ether as initiator for

**Scheme 1.** Synthetic Scheme for Substituted CL Monomer and Their Block Polymers**Figure 2.** (a) <sup>1</sup>H NMR spectrum of PEG-*b*-CPCL<sub>100</sub> and (b) MALDI-TOF-MS spectrum of TEG-CPCL<sub>50</sub>. (c) Plots of  $M_n$  determined by GPC and NMR versus the polymerization time for PEG-*b*-BuPCL<sub>50</sub>. (d) Plot of  $M_w/M_n$  versus the polymerization time for PEG-*b*-BuPCL<sub>50</sub>.

$[M_0]/[I_0] = 50$ , and these details are also given in the Supporting Information.

**Synthesis of Substituted Carboxylic Poly(caprolactone)s (PEG-*b*-CPCL<sub>x</sub>).** Trifluoroacetic acid (0.2 mL) was added slowly into PEG-*b*-CPCL<sub>100</sub> (200 mg) in dry DCM (5.0 mL), and the polymer solution was stirred at 25 °C for 30 min. The solvents were evaporated, and the polymer was redissolved in THF and precipitated in cold methanol. The purification was repeated at least twice to get pure polymer. <sup>1</sup>H NMR (400 MHz, CDCl<sub>3</sub>) δ: 4.14 (t, 2H, CH<sub>2</sub>OH), 3.84–3.64 (m, 3.8 H, PEG and OCH<sub>2</sub>), 3.57 (m, 1H, OCH), 2.56 (t, 2H, CH<sub>2</sub>COOH), 2.38 (t, 2H, COCH<sub>2</sub>), 1.99–1.67 (m, 4H, –OCH(CH<sub>2</sub>)<sub>2</sub>). FT-IR (cm<sup>-1</sup>): 3447, 2932, 2450, 1711 (C=O acid), 1355, 1257, 1175, 1096, 1059, and 955.

A similar procedure was followed for the hydrolysis of PEG-*b*-BuPCL<sub>x</sub> to produce PEG-*b*-CPCL<sub>x</sub>, where  $x = 25, 50$ , and  $75$  and also TEG-*b*-CPCL<sub>50</sub> from TEG-*b*-BuPCL<sub>50</sub>. These details are provided in the Supporting Information.

## RESULTS AND DISCUSSION

**Synthesis and Characterization of Polymers.** The synthesis of substituted caprolactone is shown in Scheme 1. A new route is developed for producing these compounds from commercially available 1,4-cyclohexanediol through multistep reactions. 1,4-Cyclohexanediol was reacted with *t*-butyl acrylate in the presence of potassium *t*-OBu via Michael reaction to produce (1) in high yield. 1 was oxidized with PCC to convert the hydroxyl group into corresponding cyclohexanone derivative (2). The compound 2 was subjected to Bayer veliger oxidation to produce substituted caprolactone monomer 3 in good yield. All of the above intermediates were completely characterized by NMR, FT-IR, and HR-MS, and their details are given in the Supporting Information.

Polyethylene glycol monomethyl ether (MW = 2000, here after referred as PEG) was employed as hydrophilic initiator for the ROP using Sn(Oct)<sub>2</sub> as a transition metal catalyst. The ratio of the Sn(Oct)<sub>2</sub> catalyst to PEG was maintained as 1:2 in mole

**Table 1.** Molecular Weights and  $[M_0]/[I_0]$  Ratio of PCL and Substituted PCL

polymer	monomer	feed $[M_0]/[I_0]$	$n^b$ (NMR)	$M_n^c$ (NMR)	$M_n^d$ (GPC)	$M_w^d$ (GPC)	$M_w/M_n^d$ (GPC)
PEG- <i>b</i> -PCL <sub>25</sub>	CL	25	29	5306	7100	8700	1.21
PEG- <i>b</i> -PCL <sub>50</sub>	CL	50	54	8156	10400	11500	1.11
PEG- <i>b</i> -PCL <sub>75</sub>	CL	75	76	10660	11500	13600	1.18
PEG- <i>b</i> -PCL <sub>100</sub>	CL	100	101	13514	23000	30000	1.31
PEG- <i>b</i> -BuPCL <sub>25</sub>	3	25	21	7418	7500	9100	1.39
PEG- <i>b</i> -BuPCL <sub>50</sub>	3	50	42	12836	9200	12900	1.22
PEG- <i>b</i> -BuPCL <sub>75</sub>	3	75	70	20060	12200	15600	1.27
PEG- <i>b</i> -BuPCL <sub>100</sub>	3	100	99	27542	18400	24900	1.35
PCL <sub>50</sub> <sup>a</sup>	CL	50	49	5754	8900	10700	1.19
BuPCL <sub>50</sub> <sup>a</sup>	3	50	46	12032	11000	14700	1.34

<sup>a</sup>Polymers are synthesized using TEG as an initiator. <sup>b</sup>The number of repeating units are determined by <sup>1</sup>H NMR. <sup>c</sup> $M_n$  was calculated based on  $M_n$  = (repeating unit mass)  $\times n$ . <sup>d</sup>Molecular weights are determined by GPC using polystyrene as a standard in THF.

ratio so that the required concentration of active initiator SnO-PEG could be generated in situ for the ROP initiation.<sup>29</sup> The monomer-to-initiator ratio was varied from  $[M_0]/[I_0] = 25, 50, 75$ , and 100 to produce different amount of carboxylic functional groups in the poly(caprolactone) diblock copolymers. The ROP was first optimized for caprolactone monomer in laboratory conditions prior to the newly designed monomer 3. Thus, the PEG-2000 initiated ROP produced two series of block copolymers PEG-*b*-PCL<sub>x</sub> and PEG-*b*-BuPCL<sub>x</sub>, where  $x$  = represents the number of repeating units in the polymers. Further, triethylene glycol monomethyl ether (TEG) was employed as an initiator to make two homopolymers TEG-PCL<sub>50</sub> and TEG-BuPCL<sub>50</sub> (these are not block copolymers). For these homopolymers, the  $[M_0]/[I_0]$  ratio was kept as 50 in the feed. The *t*-butyl ester group in the blocks of PEG-*b*-BuPCL<sub>x</sub> and homopolymer TEG-BuPCL<sub>50</sub> were hydrolyzed to obtain their corresponding carboxylic acid derivatives PEG-*b*-CPCL<sub>x</sub> and TEG-CPCL<sub>50</sub>, respectively (Bu = *t*-butyl ester and C = carboxylic acid).

The <sup>1</sup>H NMR spectrum of PEG-*b*-CPCL<sub>100</sub> is shown in Figure 2a. The protons in the repeating units are assigned with alphabets in the structure, and their corresponding peaks are indicated in the spectrum. In Figure 2a,  $-\text{OCH}_2\text{CH}_2\text{O}-$  in the PEG part (proton-b) appeared at 3.65 ppm, and upon polymerization a new ester peak appeared at 4.05 ppm (proton a); all other CL repeating unit protons appeared with respect to the expected structure. A similar NMR analysis was done for other samples to confirm their structure, and these details are given in the Supporting Information (see SF-1–SF-4). The intensity of the proton-a increased with the increase in the ratio of  $[M_0]/[I_0]$  in the feed (see SF-1 and SF-2). The comparison of the peak intensities of the PEG part (proton-b at 3.65 ppm) and the CL repeating units (protons at 4.05 ppm) gave the number average degree of polymerization,  $n = 99$  in the present case. Similarly, the  $n$  values for PEG-*b*-PCL<sub>x</sub> and PEG-*b*-CPCL<sub>x</sub> were determined, and these values are summarized in Table 1. The plot of  $n$  in the copolymer versus the  $[M_0]/[I_0]$  in the feed showed a linear trend for both PEG-*b*-PCL<sub>x</sub> and PEG-*b*-BuPCL<sub>x</sub> series (see SF-5). The plot for monomer consumption versus time also showed a linear trend (see SF-6) which again confirmed the controlled polymerization kinetics for the substituted CL monomer.<sup>28</sup>

MALDI-TOF is a powerful tool for the end group analysis of new polymers. For this purpose, the TEG initiated homopolymers TEG-PCL<sub>50</sub> and TEG-CPCL<sub>50</sub> were subjected for the MALDI-TOF analysis. MALDI-TOF MS spectra of the TEG-CPCL<sub>50</sub> is shown in Figure 2b (see SF-7 for TEG-PCL<sub>50</sub>). In

Figure 2b, the peaks were well-separated by 202 amu with respect to carboxylic caprolactone repeating unit mass. The peaks followed the sequence  $P_n = \text{MeO-TEG} + (202)_n + \text{Na}^+$  which confirmed the formation of expected polymer structure by ROP. Further, the MALDI-TOF mass spectra did not show peaks with respect to the presence of catalyst or other impurities<sup>30</sup> at the chain ends indicating the formation of high-purity polymer.

The molecular weights of the polymers were determined by gel permeation chromatography using polystyrene standards. All of the polymers showed monomodal (see SF-8) distribution and their  $M_n$ ,  $M_w$ , and polydispersites ( $M_w/M_n$ ) are summarized in Table 1. The  $M_n$  of the polymers increased with the increase in the  $[M_0]/[I_0]$  ratio in the feed in both PEG-*b*-PCL<sub>x</sub> and PEG-*b*-BuPCL<sub>x</sub> series. Further the polydispersites of the polymers were also relatively low, <1.4, confirming the formation of well-defined homogeneous polymer in the ROP process. To further understand the ROP capability of a newly synthesized monomer, a detailed ROP kinetics was carried out for both CL and the new monomer 3. For this purpose PEG was used as an initiator, and the  $[M_0]/[I_0]$  ratio was fixed as 50. These kinetic reactions were performed for 48 h, and samples were retrieved at various time intervals. The polymer samples were precipitated in methanol, and the samples were subjected to both GPC and <sup>1</sup>H NMR to determine their molecular weights and the degree of polymerization ( $n$ ). The GPC plots (see SF-9) and molecular weight details of the aliquots (see Tables ST1 and ST2) are given in the Supporting Information. In both cases, the GPC plots showed monomodal distribution and also showed a gradual increase in molecular weight with reaction time. The  $M_n$  and polydispersities of these kinetic samples were plotted against the polymerization reaction time for new monomer 3 and shown in Figure 2c and d, respectively (see SF-10 for CL monomer). The  $M_n$  obtained from GPC was found to be slightly higher compared to NMR data, indicating a slight over estimation of molecular weights by GPC. The  $M_n$  linearly increased with the reaction time and the polydispersites of the samples were obtained below 1.4, indicating their narrow molecule weight distributions. These results are almost identical to CL monomer under identical conditions. Hence, it may be concluded that newly designed carboxylic functionalized caprolactone monomer 3 is very good for producing controlled molecular weights under control ROP kinetics, similar to that of caprolactone monomer.<sup>31</sup>

**Self-Assemblies of Substituted PCL.** The newly designed PEG-*b*-BuPCL<sub>x</sub> polymers have unique features of amphiphilic

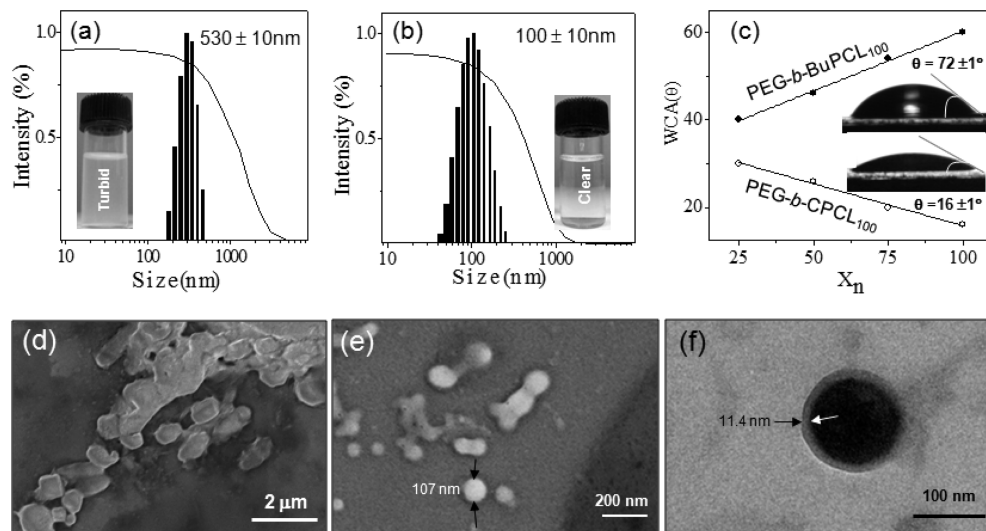


**Figure 3.** (a) DLS histogram of PEG-*b*-BPCL<sub>100</sub> in distilled water (pH = 6.0). (b) DLS histogram of PEG-*b*-CPCL<sub>100</sub> in phosphate buffer (pH = 6.0). The concentration of polymer is 0.5 mg/mL at 25 °C. (c) Plot of water contact angle (WCA) versus the “*n*” in the copolymer and the photographs showed the water droplet. (d) FE-SEM images of PEG-*b*-BPCL<sub>100</sub> and (e) PEG-*b*-CPCL<sub>100</sub>. (f) HR-TEM image of PEG-*b*-CPCL<sub>100</sub>.

A–B diblocks with hydrophilic PEG and hydrophobic carboxylic substituted PCL chains. To determine the self-assembled structures in water, they were subjected to dynamic light scattering (DLS) measurement. The DLS histogram of two diblocks PEG-*b*-BuPCL<sub>100</sub> and its carboxylic derivative PEG-*b*-CPCL<sub>100</sub> are shown in Figure 3a and b, respectively. DLS histograms of other diblocks PEG-*b*-PCL<sub>x</sub>, PEG-*b*-BuPCL<sub>x</sub>, and PEG-*b*-CPCL<sub>x</sub> are provided in the Supporting Information (see SF-11–SF-14). PEG-*b*-PCL<sub>x</sub> and PEG-*b*-BuPCL<sub>x</sub> were found to be partially soluble in water and produced turbid solution, whereas the carboxylic functionalized block PEG-*b*-CPCL<sub>x</sub> was freely dispersible in water (see vials in Figure 3a and b). DLS histogram of PEG-*b*-BuPCL<sub>100</sub> showed a bimodal distribution with an average size of 530 ± 10 nm, whereas PEG-*b*-CPCL<sub>100</sub> showed uniform monomodal distributions with average sizes of 100 ± 10 nm. The hydrodynamic radius of the nanoaggregates ( $R_h$ ) was calculated as 51 nm (half of the vesicular diameter). Static light scattering analysis of the samples (see SF-15) provided the radiation of gyration of polymer assemblies ( $R_g$ ) from the slope of Guinier plot as 50 nm (see Figure 4c). The ratio of  $R_g/R_h$  was obtained as 0.98 which suggested the existence of vesicular geometry in the PEG-*b*-CPCL<sub>100</sub>.<sup>32</sup>

Water contact angle (WCA) measurements provide direct information on the hydrophilic or hydrophobic nature of amphiphilic polymers.<sup>33</sup> WCA for the newly synthesized block polymers PEG-*b*-BuPCL<sub>100</sub> (d) and PEG-*b*-CPCL<sub>100</sub> were determined by the sessile drop method. The photographs of water droplets on the polymer film (on glass substrate) are shown in Figure 3c along with their contact angles (see SF-16 for PEG-*b*-PCL<sub>x</sub> and other samples). PEG-*b*-BuPCL<sub>x</sub> series showed an increase in the WCA with an increase in the number of caprolactone units in the diblocks. The WCA for PEG-*b*-BuPCL<sub>x</sub> series were found to be 40–60° with respect to hydrophobicity in nature. A similar trend was also observed in the PEG-*b*-PCL<sub>x</sub> (see SF-17). This indicated that the hydrophobicity of the block copolymers increased with increases in the butyl-substituted units (or normal caprolactone unit). On the other hand, the carboxylic acid functionalized diblock PEG-*b*-CPCL<sub>x</sub> series showed excellent hydrophilicity

with the WCA less than 30°.<sup>33c</sup> The increase in the hydrophilicity in PEG-*b*-CPCL<sub>x</sub> enhanced their water solubility as well as the formation of stable nanoaggregates.

The morphologies of the PEG-*b*-PCL<sub>100</sub> and PEG-*b*-CPCL<sub>100</sub> nanoaggregates were analyzed by electron microscopes. Field-emission scanning electron microscopy (FE-SEM) images of these diblock aggregates are shown in Figure 3d and e (other samples are shown in SF-18). PEG-*b*-CPCL<sub>100</sub> appeared as 107 ± 5 nm soft spherical objects (Figure 5d) and resembles morphology of polymer vesicles, whereas PEG-*b*-BuPCL<sub>100</sub> showed the formation of larger particles of 0.5 μm in size. The sizes of self-assembled aggregates in DLS are in very good agreement with the sizes of the FE-SEM images. To further confirm the existence of the vesicle in PEG-*b*-CPCL<sub>100</sub> sample, it was subjected to a high-resolution transmission electron microscope (HR-TEM). To visualize more clearly the vesicle structure in the block copolymers, the samples were stained using uranyl acetate following the reported procedure.<sup>34</sup> In Figure 3f (see more HR-TEM images in SF-19), the vesicles were appeared as a spherical object having a hydrophilic layer of 11.4 nm thickness with distinct inner cavity. Thus, the HR-TEM confirmed the formation of vesicular structures in PEG-*b*-CPCL<sub>100</sub>. Thus, the carboxylic acid PCL diblocks are very unique and capable of self-assembling into nanovesicular scaffolds in water.

**Encapsulation Capabilities of PCL Vesicles.** Vesicles are unique self-assembled structures for dual loading of hydrophobic and hydrophilic molecules in the layer and core, respectively.<sup>13c</sup> To study the loading capabilities of carboxylic PCL vesicles, water-soluble Rhodamine-B (Rh-B) and water insoluble drugs ibuprofen (IBU, anti-inflammatory drug) and camptothecin (CPT, anticancer drug) were chosen. In the present studies three types of loaded vesicles are produced from PEG-*b*-CPCL<sub>100</sub> diblock: (i) hydrophilic molecule Rh-B loaded vesicle ( $V_{Rh-B}$ ); (ii) hydrophobic drug-loaded vesicles  $V_{IBU}$  and  $V_{CPT}$ ; and (iii) hydrophilic + hydrophobic dual-loaded vesicle  $V_{Rh+IBU}$ . Rh-B encapsulation is one of the most important control experiments to prove the existence of vesicular scaffolds in polymer assemblies.<sup>13c</sup> For example, micelles or nanoparticles cannot encapsulate the water-soluble

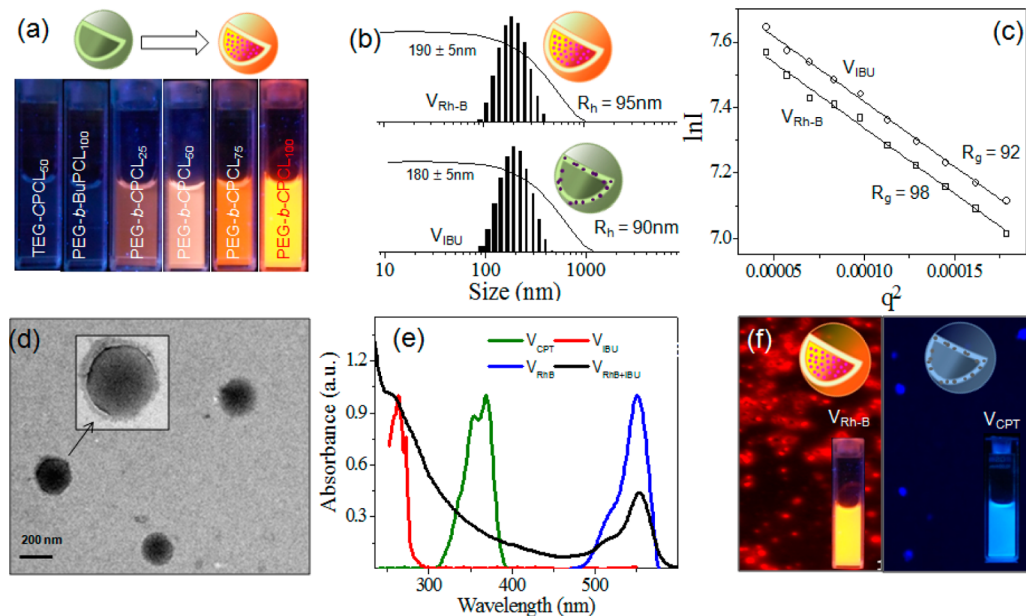


**Figure 4.** (a) Photographs of vials contain the polymers after the Rh–B encapsulation. (b) DLS histograms of  $V_{Rh\text{-}B}$  and  $V_{IBU}$ . (c) SLS plot for  $V_{Rh\text{-}B}$  and  $V_{IBU}$ . (d) HR-TEM image of  $V_{Rh\text{-}B}$ . (e) Absorbance spectra of loaded vesicles. (f) FL microscope images of  $V_{Rh\text{-}B}$  and  $V_{CPT}$ .

Rh–B since their internal part is hydrophobic. PEG-*b*-BuPCL<sub>100</sub>, PEG-*b*-CPCL<sub>100</sub> and TEG-CPCL<sub>50</sub> were subjected to Rh–B encapsulation in water (see experimental section for more details). The photographs of the Rh–B encapsulated samples in vials after dialysis are shown in Figure 4a (photographs captured under hand-held UV-light exposure). As it can be clearly evident that the carboxylic PCL block copolymer showed the stable encapsulation of Rh–B, whereas its butyl ester and homopolymer TEG-CPCL<sub>50</sub> did not stabilize Rh–B. This observation confirmed that the diblock nature as well as the presence of carboxylic functional groups is essential to produce stable PCL vesicles in water.

The PCL loaded vesicles were further characterized by dynamic and static light scattering methods, and their data are shown in Figure 4b and c, respectively. The hydrodynamic diameter of the Rh–B encapsulated vesicle was determined from DLS as 190 nm (see Figure 4b). The slight increase in size in the Rh–B vesicles compared to the nascent vesicle (see Figure 3b) is attributed to the occupation of the guest molecules in the vesicular assemblies.<sup>13c,34a</sup> The hydrodynamic radius of the Rh–B loaded vesicle ( $R_h$ ) was calculated as 95 nm. Static light scattering provided the radiation of gyration of vesicular assemblies ( $R_g$ ) as 98 nm (see Figure 4c). The ratio of  $R_g/R_h$  was obtained as 1.03 which confirmed the existence of vesicular geometry in Rh–B loaded samples.<sup>30</sup> In a similar way IBU loaded vesicles were also analyzed. The hydrodynamic diameter of the IBU encapsulated vesicles was determined as 180 nm from DLS (see Figure 4b). The ratio of  $R_g/R_h$  was obtained as 1.02 for IBU loaded vesicles. HR-TEM images of Rh–B loaded vesicles are shown in Figure 4d. These smooth spherical objects with 200 nm showed the formation of vesicular assemblies. The HR-TEM image of IBU loaded sample also confirmed the existence of the vesicular assemblies (see SF 18). Similarly, the self-assemblies of  $V_{CPT}$  and  $V_{Rh\text{-}B+IBU}$  dual loaded vesicles were also confirmed, and their details are given in the Supporting Information (see SF-18, SF-20, and SF-21).

Drug loading contents (DLC) of the vesicles were determined by absorbance spectroscopy. Absorbance spectra of drug loaded scaffolds are shown in Figure 4e. The unloaded vesicular scaffold showed absorbance maxima at 190 nm (see SF-22) which does not interfere with the drug molecules absorbance in the visible region. The  $V_{Rh\text{B}}$  showed absorbance maxima at 555 nm, and IBU  $V_{IBU}$  showed absorbance maxima at 265 nm. In case of dual loaded vesicles ( $V_{Rh\text{-}B+IBU}$ ), peaks for Rh–B and IBU are clearly visible. The camptothecin (CPT) loaded vesicles ( $V_{CPT}$ ) showed absorbance maxima at 365 nm. Based on the molar extinction coefficient of Rh–B, IBU, and CPT, the drug loading content of individual vesicles were determined as 1.1%, 9.5%, and 1.2% for  $V_{Rh\text{B}}$ ,  $V_{IBU}$ , and  $V_{CPT}$ , respectively. The loading contents of Rh–B and IBU were determined as 1.7% and 13% in the dual loaded  $V_{Rh\text{B+IBU}}$  vesicle, respectively. In similar way drug loading efficiencies were also calculated for individual vesicles as 11%, 32%, and 12% for  $V_{Rh\text{B}}$ ,  $V_{IBU}$ , and  $V_{CPT}$ , respectively. The loading efficiency of Rh–B and IBU were determined as 17% and 51% in the dual-loaded  $V_{Rh\text{B+IBU}}$  vesicle, respectively. Among all of the loaded molecules, IBU showed a higher loading ability, and this was attributed to its smaller molecular size. The Rh–B and CPT are fluorescent molecules as a result their vesicles  $V_{Rh\text{B}}$  and  $V_{CPT}$  were also found to be highly fluorescent. Fluorescent microscope images of these vesicles are shown in Figure 4f. The  $V_{Rh\text{B}}$  showed red fluorescence, whereas  $V_{CPT}$  was found to be blue luminescent. The fluorescent maxima of loaded vesicles clearly matched with the appearance of red and blue luminescence in  $V_{Rh\text{B}}$  and  $V_{CPT}$ , respectively (see SF-23).

#### pH Response and Zeta Potential of the PCL Vesicles.

Zeta potential measurement is very important tool for understanding the solution dynamic of charged aggregates or more likely self-assemblies of anionic (or cationic) polymeric nanostructures.<sup>31</sup> In solution electrically charged species (nano-assemblies) tend to move under the effect of electrical field; thereby the zeta potential of the spherical aggregates was expected to show significant change with pH of media. The custom designed PEG-*b*-CPCL<sub>x</sub> vesicles have carboxylic acid

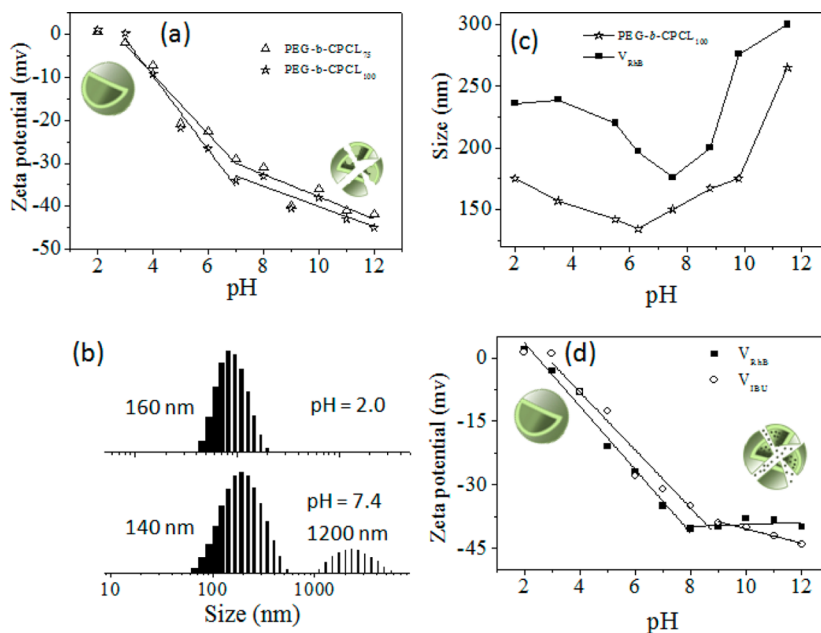


**Figure 5.** (a) Zeta potential of PEG-*b*-CPCL<sub>x</sub> in various pH (0.5 mg/mL) at 25 °C. (b) DLS histograms of PEG-*b*-CPCL<sub>100</sub> in pH = 2.0 and 7.4. (c) Size of the PEG-*b*-CPCL<sub>100</sub> and V<sub>Rh-B</sub> in various pH (0.5 mg/mL) at 25 °C. (d) Zeta potential of V<sub>Rh-B</sub> and V<sub>IBU</sub> in various pH (0.5 mg/mL) at 25 °C.

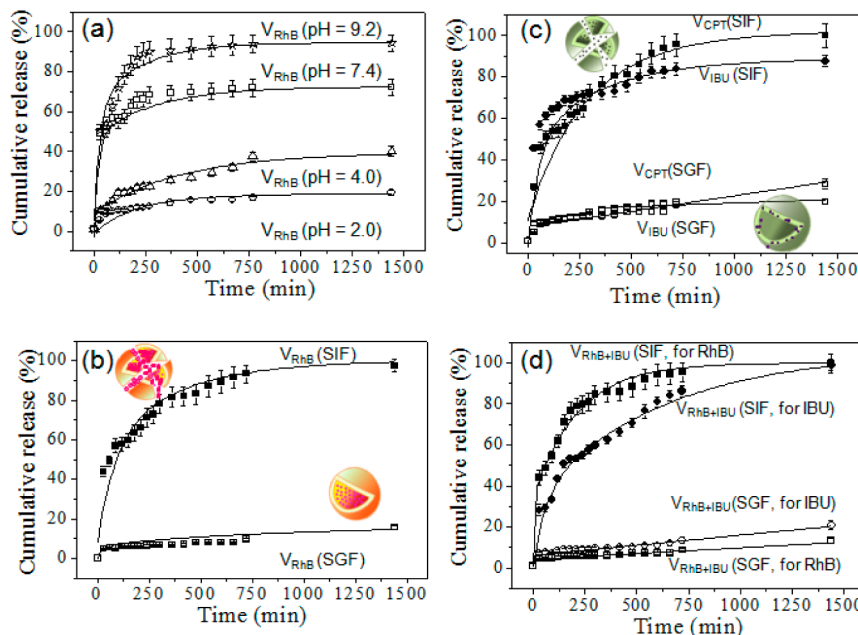


**Figure 6.** (a) Cumulative release of V<sub>Rh-B</sub> in various pH buffers at 37 °C. (b) Cumulative release of V<sub>Rh-B</sub> in SIF and SGF at 37 °C. (c) Cumulative release of V<sub>IBU</sub> and V<sub>CPT</sub> (c) in SIF and SGF at 37 °C. (d) Cumulative release of dual-loaded vesicle V<sub>Rh-B+IBU</sub> in SIF and SGF at 37 °C.

functional group anchored on the PCL backbone; as a result they were expected to show significant change in the self-assemblies with respect to the pH of the solution. Zeta potentials of the PEG-*b*-CPCL<sub>x</sub> vesicles ( $x = 75$  and  $100$ ) were plotted against various pH values and presented in Figure 5a (see PEG-*b*-CPCL<sub>25</sub> and PEG-*b*-CPCL<sub>50</sub> in SF-24). The zeta potential of the vesicles increased (more negative potential) with the increase in the pH as the carboxylic acid group became a carboxylate anion at higher pH. The plots showed a fast increase up to pH~ 7.0 (0 to -30 mV), and thereafter the increase was not so significant (-30 to -40 mV). This suggested that vesicular assemblies underwent structural

changes from acidic to neutral pH, whereas the structural change was less significant from neutral to basic pH.

To trace these structural changes in the vesicular assemblies, the size of the aggregates was also measured by DLS at various pH. DLS histograms of PEG-*b*-CPCL<sub>100</sub> at pH = 2.0 and 7.4 are shown in Figure 5b. The vesicles showed a monomodal distribution at pH = 2.0, whereas a broad bimodal distribution was obtained with higher sizes at basic pH = 7.4 (see other vesicles in SF-25). In Figure 5c, the plots showed the size of aggregates at various pH. The size of the aggregates did not change up to pH = 6 which suggest that the vesicles are stable in the region pH < 6.0, and a further increase in pH produced

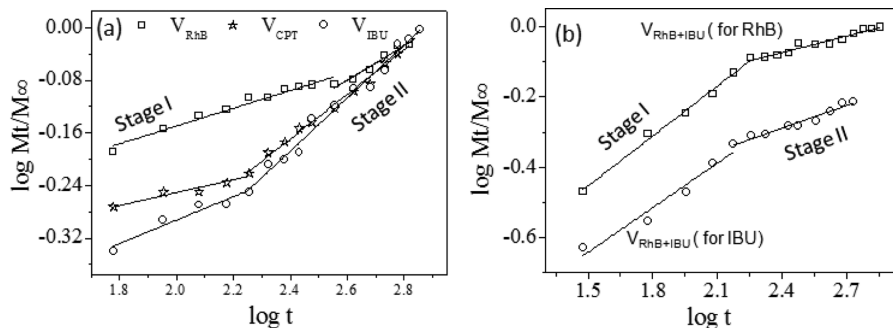


**Figure 7.** Plots of the  $\log(M_t/M_\infty)$  versus  $\log t$  for individual loaded vesicles (a) and dual-loaded vesicles (b).

**Table 2. Release Kinetic Parameters of Vesicles**

sample	stage I			stage II		
	n	k	$R^2$	n	k	$R^2$
VRh-B	0.134	0.381	0.962	0.262	0.173	0.946
VIBU	0.178	0.224	0.921	0.402	0.071	0.980
VCPT	0.097	0.363	0.909	0.338	0.104	0.990
dual (for Rh-B)	0.473	0.078	0.991	0.156	0.356	0.945
dual (for IBU)	0.422	0.053	0.945	0.215	0.156	0.960

larger size particles with respect to the breakage of the vesicular scaffold. To further confirm this trend, the polydispersity index (PDI) from DLS data are plotted against the variation of pH (see Supporting Information SF-26a). The plots showed a nonlinear trend in the polydispersity with pH and as observed in Figure 5c. The PDI of the aggregates were found to be  $<0.12$  for the pH = 2.0–6.0, and the values increased to 0.45–0.63 above pH > 7.0. The number average data (see SF-26b) were also found to be similar to that of intensity as shown in Figure 5c. These two parameters clearly confirmed the cleavage of the vesicular assemblies preferable at neutral-to-basic pH.

This trend in the zeta potential (in Figure 5a) and increases in the size of the polymer aggregates (Figure 5c) was attributed to the disassembly of PCL vesicles at higher pH. The carboxylate anions at higher pH repelled the hydrophobic layer apart which induced the disassembly. A similar trend was recently observed by Do et al.<sup>35</sup> in PEG-polyacrylic acid self-assembly. VRhB and VIBU loaded vesicles were also subjected for zeta potential, and their data are shown in Figure 5d. These cargo-loaded vesicles were also showed a nonlinear trend in their zeta potential as similar to that of unloaded vesicles (see Figure 5a). The size of the VRhB also increased at higher pH with respect to the breakage of the vesicular structure (see Figure 5c). This confirmed that the pH responsive nature of the PCL vesicles not disturbed by the loaded drug in their layer or inside the vesicle. Thus, this custom-designed PCL block copolymers are unique pH responsive vesicles, and they are able to stabilize the hydrophilic as well as hydrophobic molecules (or drugs) in strong acidic media (below pH < 2.0) and capable of selectively rupture to delivery them at neutral or higher pH.

**In Vitro Delivery under the Simulated GI Tract.** Oral drug delivery capability of PCL vesicular assemblies were tested under in vitro conditions. The release characteristics of VRh-B at 37 °C at various pH = 2.0, 4.0, 7.4, and 9.2 are shown in Figure 6. The cumulative releases of the Rh-B releases were estimated by absorbance spectroscopy (see SF-27), and these are plotted and shown in Figure 6a. It can be evident that the vesicles were stable in strong acidic conditions (pH = 2.0) and only less than

15 ± 3% of the loaded Rh-B content was released up on 24 h. At pH = 4.0, the releasing ability slightly increase to reach 30 ± 6%. At neutral pH = 7.4, the vesicles underwent burst release in a short period of 4 h, and thereafter, the controlled release continued to 70 ± 7% until 24 h. At basic pH = 9.2, the release profile increased further, and all of the loaded cargoes (89 ± 9%) were released. This variable pH release kinetics clearly demonstrates the ability of the newly designed carboxylic functionalized PCL vesicles under a controlled manner with respect to the pH of the environment. To study the release kinetics of these PCL vesicles under GI tract, they were subjected to freshly prepared simulated gastric fluid (SGF, pH = 2.0) and simulated interstitial fluid (SIF, pH = 7.4) as per the literature reports.<sup>7</sup> Figure 6b showed the release kinetics of the VRhB loaded vesicles under SGF and SIF. The vesicles were very stable in SGF, whereas they completely broke to release the 90 ± 8% of the Rh-B in SIF. In Figure 6c, the hydrophobic drug loaded vesicles VIBU and VCPT also showed similar burst release of the loaded drugs selectively in SIF. In Figure 6d, the hydrophilic and hydrophobic dual loaded vesicle VIBU+RHb was also found to show selective release in SIF as similar to their individual counterparts. The above in vitro studies summarized that loaded PCL vesicles were stabilized in the gastric conditions and selectively collapse to release at interstitial pH.

The release kinetics of loaded molecules (or drugs) in the polymer matrix is a complex problem and not clearly understood to date. Peppas and co-workers<sup>36</sup> proposed the following semiempirical model for the polymer drug releases either by diffusion, erosion, or a combination of both processes:

$$M_t/M_\infty = kt_n \quad (\text{or}) \quad \log(M_t/M_\infty) = n \log t + \log k$$

where  $M_t$  and  $M_\infty$  are cumulative releases of loaded cargoes (or drugs) at time  $t$  and infinite,  $n$  is a release exponent, and  $k$  is the rate constant. The  $n$ -value provides direct information on the release kinetics either by Fickian diffusion ( $n = 0.43$ ) or non-Fickian mechanism ( $n < 0.43$ ) in which both diffusion and erosion occurred together.<sup>32</sup> This kinetic methodology was recently employed by Sanson et al.<sup>17</sup> and Yang et al.<sup>7</sup> independently in the release studies of hydrophilic or

hydrophobic drugs. Since the present investigation provides unique opportunity to load both hydrophilic and hydrophobic in a single PCL vesicles, it would be important to understand their release pattern under SIF conditions. The release profiles of  $V_{IBU}$ ,  $V_{RhB}$ ,  $V_{CPT}$ , and  $V_{IBU+RhB}$  under SIF at 7.4 were subjected to the above kinetics. The plots of the  $\log(M_t/M_\infty)$  versus  $\log t$  for the deliveries of Rh-B, IBU, CPT, or IBU+Rh-B are shown in Figure 7. The individual loaded vesicles  $V_{IBU}$ ,  $V_{RhB}$ , and  $V_{CPT}$  showed release in two stages. These data were fitted with linear plot to obtain their  $n$  and their  $k$ -values from the slope and intercepts, respectively. These values are summarized in Table 2.

The individual loaded vesicles showed relatively low  $n$  values ( $n < 0.2$ ) in stage I with respect to the 60% drug release. This was attributed to both diffusion and erosion mechanisms. The increase in the  $n$ -values ( $0.2 < n < 0.4$ ) in stage II indicated that the remaining 40% of the drugs were released through diffusion process. It is very important to note that the release kinetics of individual vesicles showed identical release patterns for both hydrophilic and hydrophobic cargoes. Thus, the vesicles are potential drug loading vectors for releasing both water-soluble and water-insoluble drugs under the identical rate in a single scaffold. On the other hand, the release kinetics of the drugs (or Rh-B) from the dual loaded vesicles were followed just opposite compared to their individual counterparts. Both IBU and Rh-B were released with large  $n$ -values ( $n \leq 4.3$ ) in the stage I compared to stage II ( $n < 0.21$ ). This revealed that the dual-loaded vesicles first release its 60% of the drugs predominately by diffusion controlled process rather than diffusion + erosion. Though both individual and dual loaded vesicles followed a similar two-stage kinetics, the “ $n$ ” values revealed that the process in which the cargoes release seems to be different. The dual-loaded vesicles released 60% of the drug by diffusion process, whereas the vesicles with individual drugs predominantly followed the combination of diffusion plus erosion. It suggested that the dual loading provide more stability in the vesicular assemblies which is less influenced by the erosion process. The present investigation provide first time insight into the concept of the dual drug delivery based on PCL vesicles for drugs (like CPT and IBU) and water-soluble Rh-B molecules under the GI tract. Though the approach demonstrated here tested only few examples, it is not restricted to few cases, and in general, it is applicable to wide range of drugs which are yet to be explored in oral drug delivery.

## CONCLUSION

In conclusion, the present investigation has successfully demonstrated the creation of pH-responsive PCL vesicles and their loading and releasing capabilities of hydrophobic and hydrophilic molecules under a stimulated GI tract. A new carboxylic functionalized caprolactone monomer was designed and synthesized for the above purpose readily from commercial starting materials and polymerized under ROP. The carboxylic substituted PCL block copolymers PEG-*b*-CPCL<sub>x</sub> were very unique in producing water-soluble nanometer sized vesicles. The existence of the PCL vesicle was confirmed by various techniques such as DLS, SLS, FE-SEM, HR-TEM, WCA, and so on. Zeta potential and DLS studies revealed that pH-responsive PCL vesicles found to be stable up to pH < 6.0, and they rupture to release the loaded drug molecules at the neutral or pH > 7.0. The loading and delivering capabilities were investigated for water-soluble molecules such as Rh-B and hydrophobic drugs like IBU or CPT. The in vitro release

characteristics revealed that the PCL vesicles exclusively release the drugs only under SIF which is identical to our physiological conditions of small intestine. Further, the custom designed PEG-*b*-CPCL<sub>x</sub> block copolymers provide a new opportunity to tag either drug molecules or antibody for site-directed delivery in PCL systems while retaining the pH as stimuli for release. The carboxylic acid group either may be partially or fully substituted with suitable chemical functional groups for application as scaffolds for stabilizing metal nanoparticles. The nanoparticles along with drug conjugates may provide new opportunity for real time imaging or delivery to specific tumor site and so on. Currently efforts are taken to employ these pH response PCL vesicles for delivery of anticancer drugs in collaboration with biology research groups which will be published elsewhere.

## ASSOCIATED CONTENT

### Supporting Information

NMR and GPC chromatograms of diblock polymers (PEG-*b*-PCL<sub>x</sub>, PEG-*b*-BuPCL<sub>x</sub>, and PEG-*b*-CPCL<sub>x</sub>) and homopolymers (TEG-PCL<sub>50</sub>, TEG-BuPCL<sub>50</sub>, and TEG-CPCL<sub>50</sub>), kinetic studies of ROP for caprolactone and  $\gamma$ -substituted caprolactone, DLS histograms for all polymers, WCA measurement images for diblock polymers, FESEM image of  $V_{RhB}$ ,  $V_{IBU}$ ,  $V_{CPT}$ , and  $V_{RhB+IBU}$ , HRTEM image of  $V_{IBU}$ , TGA profiles of diblock and homopolymers, Rh-B absorbance spectra with various concentrations,  $V_{IBU}$ ,  $V_{CPT}$  fluorescence spectra, DSC thermograms of diblock and homopolymers, and vesicular stability of PEG-*b*-CPCL<sub>75</sub> at various pH. CAC calculation for PEG-*b*-PCL<sub>100</sub> blocks. This material is available free of charge via the Internet at <http://pubs.acs.org>.

## AUTHOR INFORMATION

### Corresponding Author

\*E-mail: jayakannan@iiserpune.ac.in. Fax: +91-20-2590 8187.

### Notes

The authors declare no competing financial interest.

## ACKNOWLEDGMENTS

The authors thank research grant from Department of Science and Technology (DST), New Delhi, India, under nanomission initiative project SR/NM/NS-42/2009 and SERC scheme project SR/S1/OC-54/2009. B.S. thanks CSIR, New Delhi, India for research fellowship.

## REFERENCES

- (1) Al-Hilal, T. A.; Alam, F.; Byun, Y. *Adv. Drug Delivery Rev.* **2013**, *65*, 845–864.
- (2) Ensign, L. M.; Cone, R.; Hanes, J. *Adv. Drug Delivery Rev.* **2012**, *64*, 557–570.
- (3) (a) Gao, W.; Chan, J. M.; Farokhzad, O. C. *Mol. Pharmaceutics* **2010**, *7*, 1913–1920. (b) Huang, Y.; Tang, Z.; Zhang, X.; Yu, H.; Sun, H.; Pang, X.; Chen, X. *Biomacromolecules* **2013**, *14*, 2023–2032. (c) Mandracchia, D.; Pitarresi, G.; Palumbo, F. S.; Carlisi, B.; Giannonna, G. *Biomacromolecules* **2004**, *5*, 1973–1982. (d) Paliwal, R.; Paliwal, S. R.; Agrawal, G. P.; Vyas, S. P. *Mol. Pharmaceutics* **2011**, *8*, 1314–1321. (e) Casadei, M. A.; Pitarresi, G.; Calabrese, R.; Paolicelli, P.; Giannonna, G. *Biomacromolecules* **2008**, *9*, 43–49.
- (4) (a) Kim, H.; Kang, Y. J.; Kang, S.; Kim, K. T. *J. Am. Chem. Soc.* **2012**, *134*, 4030–4033. (b) Rodríguez-Hernández, J.; Lecommandoux, S. *J. Am. Chem. Soc.* **2005**, *127* (7), 2026–2027. (c) Klaikherd, A.; Nagamani, C.; Thayumanavan, S. *J. Am. Chem. Soc.* **2009**, *131*, 4830–4838.

- (5) (a) Kim, K. T.; Cornelissen, J. J. L. M.; Nolte, R. J. M.; Hest, J. C. M. v. *J. Am. Chem. Soc.* **2009**, *131*, 13908–13909. (b) Krannig, K.-S.; Schlaad, H. *J. Am. Chem. Soc.* **2012**, *134*, 18542–18545. (c) Su, J.; Chen, F.; Cryns, V. L.; Messersmith, P. B. *J. Am. Chem. Soc.* **2011**, *133*, 11850–11853. (d) Griset, A. P.; Walpole, J.; Liu, R.; Gaffey, A.; Colson, Y. L.; Grinstaff, M. W. *J. Am. Chem. Soc.* **2009**, *131*, 2469–2471. (e) Lee, S.-M.; Chen, H.; Dettmer, C. M.; O'Halloran, T. V.; Nguyen, S. T. *J. Am. Chem. Soc.* **2007**, *129*, 15096–15097.
- (6) Fuhrmann, G.; Grotzky, A.; Lucic, R.; Mattoori, S.; Yu, H.; Zhang, B.; Walde, P.; Schluter, A. D.; Gauthier, M. A.; Leroux, J.-C. *Nat. Chem.* **2013**, *5*, 582–589. (b) Gillies, E. R.; Frechet, J. M. J. *Bioconjugate Chem.* **2005**, *16*, 361–368.
- (7) Yang, Y. Q.; Guo, X. D.; Lin, W. J.; Zhang, L. J.; Zhang, C. Y.; Qian, Y. *Soft Matter* **2012**, *8*, 454–464.
- (8) (a) Yang, Y. Q.; Lin, W. J.; Zhao, B.; Wen, X. F.; Guo, X. D.; Zhang, L. J. *Langmuir* **2012**, *28*, 8251–8259. (b) Du, Y.; Chen, W.; Meng, F.; Zhong, Z. *Biomaterials* **2012**, *33*, 7291–7299.
- (9) Roger, E.; Kalscheuer, S.; Kirtane, A.; Guru, B. R.; Grill, A. E.; Whittum-Hudson, J. *Mol. Pharmaceutics* **2012**, *9*, 2103–2110.
- (10) (a) Felber, A. E.; Dufresne, M.-H.; Leroux, J.-C. *Adv. Drug Delivery Rev.* **2012**, *64*, 979–992.
- (11) (a) Du, J.; Tang, Y.; Lewis, A. L.; Armes, S. P. *J. Am. Chem. Soc.* **2005**, *127*, 17982–17983. (b) Du, J.; Armes, S. P. *J. Am. Chem. Soc.* **2005**, *127*, 12800–112801. (c) Zhu, L.; Zhao, L.; Yang, Z. *Langmuir* **2012**, *28*, 11988–11996. (d) Zhang, J.; Wu, L.; Wang, Z.; Deng, C.; Liu, H.; Zhong, Z. *Langmuir* **2012**, *28*, 2056–2065. (e) Du, J.; Fan, L.; Liu, Q. *Macromolecules* **2012**, *45*, 8275–8283. (f) Blanazs, A.; Massignani, M.; Armes, S. P. *Adv. Funct. Mater.* **2009**, *19*, 2906–2914.
- (12) (a) Sanson, C.; Diou, O.; Thévenot, J.; Ibarboure, E.; Soum, A.; Brûlet, A.; Miraux, S.; Thiaudière, E.; Tan, S.; Brisson, A.; Dupuis, V.; Sandre, O.; Lecommandoux, S. *ACS Nano* **2011**, *5*, 1122–1140. (b) Sanson, C.; Schatz, C.; Le Meins, J.-F. O.; Brûlet, A.; Soum, A.; Lecommandoux, S. *Langmuir* **2009**, *26*, 2751–2760.
- (13) (a) Gaitzsch, J.; Appelhans, D.; Wang, L.; Battaglia, G.; Voit, B. *Angew. Chem., Int. Ed.* **2012**, *51*, 4448–4451. (b) Versluis, F.; Tomatsu, I.; Fregunese, C.; Tepper, A. W. J. W.; Staart, M. C. A.; Kros, A. *J. Am. Chem. Soc.* **2009**, *131*, 13186–13187. (c) Pramod, P. S.; Takamura, K.; Chapekar, S.; Balasubramanian, N.; Jayakannan, M. *Biomacromolecules* **2012**, *13*, 3627–3640.
- (14) Loamas, H.; Canton, I.; MacNiel, S.; Du, J.; Armes, S. P.; Ryan, A. J.; Lewis, A. L.; Battaglia, G. *Adv. Mater.* **2007**, *19*, 4238–4243.
- (15) Popescu, M.-T.; Tsitsilianis, C. *ACS Macro Lett.* **2013**, *2*, 222–225.
- (16) (a) Yang, X.; Grailer, J. J.; Rowland, I. J.; Javedi, A.; Hurley, S. A.; Matson, V. Z.; Gong, S. *ACS Nano* **2010**, *4*, 6805–6817. (b) Sanson, C.; Diou, O.; Thévenot, J.; Ibarboure, E.; Soum, A.; Brûlet, A.; Miraux, S.; Thiaudière, E.; Tan, S.; Brisson, A.; Dupuis, V.; Sandre, O.; Lecommandoux, S. *ACS Nano* **2011**, *5*, 1122–1140.
- (17) Sanson, C.; Schatz, C.; Le Meins, J.-F.; Soum, A.; Thévenot, J.; Garanger, E.; Lecommandoux, S. *J. Controlled Release* **2010**, *147*, 428–435.
- (18) Jerome, C.; Lacomte, P. *Adv. Drug Delivery Rev.* **2008**, *60*, 1056–1076.
- (19) (a) Zupancich, J. A.; Bates, F. S.; Hillmyer, M. A. *Macromolecules* **2006**, *39*, 4286–4288. (b) Geng, Y.; Discher, D. E. *J. Am. Chem. Soc.* **2005**, *127*, 12780–12781.
- (20) Gou, M.; Men, K.; Shi, H.; Xiang, M.; Zhang, J.; Song, J.; Long, J.; Wan, Y.; Luo, F.; Zhao, X.; Qian, Z. *Nanoscale* **2011**, *3*, 1558–1567.
- (21) (a) Schuetz, P.; Greenall, M. J.; Bent, J.; Furzeland, S.; Atkins, D.; Butler, M. F.; McLeish, T. C. B.; Buzz, D. M. A. *Soft Matter* **2011**, *7*, 749–759. (b) Šachl, R.; Uchman, M.; Matějíček, P.; Procházka, K.; Štepánek, M.; Špírková, M. *Langmuir* **2007**, *23* (6), 3395–3400. (c) Ghorghchian, P. P.; Li, G.; Levine, D. H.; Davis, K. P.; Bates, F. S.; Hammer, D. A.; Therien, M. J. *Macromolecules* **2006**, *39*, 1673–1675. (d) Katz, J. S.; Eisenbrown, K. A.; Johnston, E. D.; Kamat, N. P.; Rawson, J.; Therien, M. J.; Burdick, J. A.; Hammer, D. A. *Soft Matter* **2012**, *8*, 10853–10862.
- (22) Chang, L.; Deng, L.; Wang, W.; Lv, Z.; Hu, F.; Dong, A.; Zhang, J. *Biomacromolecules* **2012**, *13*, 3301–3310.
- (23) (a) Cheng, Y.; Hao, J.; Lee, L. A.; Biewer, M. C.; Wang, Q.; Stefan, M. C. *Biomacromolecules* **2012**, *13*, 2163–2173. (b) Rieger, J.; Bernaerts, K. V.; Du Prez, F. E.; Jérôme, R.; Jérôme, C. *Macromolecules* **2004**, *37*, 9738–9745. (c) Hao, J.; Servello, J.; Sista, P.; Biewer, M. C.; Stefan, M. C. *J. Mater. Chem.* **2011**, *21*, 10623–10628. (d) Tian, D.; Dubois, P.; Jérôme, R. *Macromolecules* **1997**, *30*, 1947–1954.
- (24) Yao, K.; Wang, J.; Zhang, W.; Lee, J. S.; Wang, C.; Chu, F.; He, X.; Tang, C. *Biomacromolecules* **2011**, *12*, 2171–2177.
- (25) (a) Mahmud, A.; Xiong, X.-B.; Lavasanifar, A. *Macromolecules* **2006**, *39*, 9419–9428. (b) Patel, S. K.; Lavasanifar, A.; Choi, P. *Biomaterials* **2010**, *31*, 345–357.
- (26) Mahmud, A.; Patel, S.; Molavi, O.; Choi, P.; Samuel, J.; Lavasanifar, A. *Biomacromolecules* **2009**, *10*, 471–478.
- (27) (a) Riva, R.; Schmeits, S.; Jérôme, C.; Jérôme, R.; Lecomte, P. *Macromolecules* **2007**, *40*, 796–803. (b) Li, H.; Riva, R.; Jérôme, R.; Lecomte, P. *Macromolecules* **2007**, *40*, 824–831. (c) Tian, D.; Halleux, O.; Dubois, P.; Jérôme, R.; Sobry, R.; Van den Bossche, G. *Macromolecules* **1998**, *31*, 924–927.
- (28) (a) Trollsas, M.; Lee, V. Y.; Mecerreyes, D.; Lowenhielm, P.; Moller, M.; Miller, R. D.; Hedrick, J. L. *Macromolecules* **2000**, *33*, 4619–4627. (b) Trollsas, M.; Lowenhielm, P.; Lee, V. Y.; Moller, M.; Miller, R. D.; Hedrick, J. L. *Macromolecules* **1999**, *32*, 9062–9066.
- (29) Odian, G. *Principles of Polymerization*, 4th ed.; John Wiley and Sons: New York, 2004; pp 581–585.
- (30) Li, Y.; Hoskins, J. N.; Sreerama, S. G.; Grayson, S. M. *Macromolecules* **2010**, *43*, 6225–6228.
- (31) (a) Mishra, A. K.; Patel, V. K.; Vishwakarma, N. K.; Biswas, C. S.; Raula, M.; Misra, A.; Mandal, T. K.; Ray, B. *Macromolecules* **2011**, *44*, 2465–2473. (b) Kamber, N. E.; Jeong, W.; Gonzalez, S.; Hedrick, J. L.; Waymouth, R. M. *Macromolecules* **2009**, *42*, 1634–1639.
- (32) (a) Houga, C. M.; Giermanska, J.; Lecommandoux, S. B.; Borsali, R.; Taton, D.; Gnanou, Y.; Le Meins, J.-F. O. *Biomacromolecules* **2008**, *10*, 32–40. (b) Matsudo, T.; Ogawa, K.; Kokufuta, E. *Biomacromolecules* **2003**, *4*, 728–735.
- (33) (a) Seyednejad, H.; Vermonden, T.; Fedorovich, N. E.; van Eijk, R.; van Steenbergen, M. J.; Dhert, W. J. A.; van Nostrum, C. F.; Hennink, W. E. *Biomacromolecules* **2009**, *10*, 3048–3054. (b) Esteves, A. C. C.; Lyakhova, K.; van der Ven, L. G. J.; van Benthem, R. A. T. M.; de With, G. *Macromolecules* **2013**, *46*, 1993–2002. (c) Li, Y.; Peterson, J. J.; Jhaveri, S. B.; Carter, K. R. *Langmuir* **2013**, *29*, 4632–4639.
- (34) (a) Sridhar, U.; Pramod, P. S.; Jayakannan, M. *RSC Adv.* **2013**, *3*, 21237–21241. (b) Moughton, A. O.; O'Reilly, R. K. *Chem. Commun.* **2010**, *46* (7), 1091–1093. (c) Zhao, W.; Chen, D.; Hu, Y.; Grason, G. M.; Russell, T. P. *ACS Nano* **2010**, *5* (1), 486–492.
- (35) Ren, T.; Liu, Q.; Lu, H.; Liu, H.; Zhang, X.; Du, J. *J. Mater. Chem.* **2012**, *22*, 12329–12338.
- (36) (a) Siepmann, J.; Peppas, N. A. *Adv. Drug Delivery Rev.* **2001**, *48*, 139–157. (b) Young, C. R.; Dietzsch, C.; Cerea, M.; Farrell, T.; Fegely, K. A.; Rajabi-Siahboomi, A.; McGinity, J. W. *Int. J. Pharmaceutics* **2005**, *301*, 112–120. (c) Li, Y.; Li, H.; Wei, M.; Lu, J.; Jin, L. *Chem. Eng. J.* **2009**, *151*, 359–366.